Journal of Renewable Materials

Tech Science Press

DOI: 10.32604/jrm.2024.056639

ARTICLE

Graphene Oxide and *Moringa oleifera* Seed Oil Incorporated into Gelatin-Based Films: A Novel Active Food Packaging Material

María Fernanda Cardona Lunar[1], Ramón Ordoñez[2], Heidi Fonseca Florido[3], Joaquín Hernández-Fernández[4,5,6] and Rodrigo Ortega-Toro[1,*]

[1]Food Packaging and Shelf-Life Research Group (FP&SL), Food Engineering Department, University of Cartagena, Cartagena de Indias, 130015, Colombia

[2]Departamento de Ingeniería Química, Universidad Nacional Autónoma de Honduras, Tegucigalpa, 11101, Honduras

[3]Investigador por México-CONAHCYT, Centro de Investigación en Química Aplicada (CIQA), Saltillo, 25294, México

[4]Chemistry Program, Department of Natural and Exact Sciences, San Pablo Campus, University of Cartagena, Cartagena, 130015, Colombia

[5]Chemical Engineering Program, School of Engineering, Universidad Tecnológica de Bolívar, Cartagena, 130001, Colombia

[6]Department of Natural and Exact Science, Universidad de la Costa, Barranquilla, 080002, Colombia

[*]Corresponding Author: Rodrigo Ortega-Toro. Email: rortegap1@unicartagena.edu.co

Received: 27 July 2024 Accepted: 26 November 2024 Published: 20 February 2025

ABSTRACT

The extensive use of polymeric materials in single-use packaging has driven the need to develop biodegradable alternatives. This study investigates the incorporation of graphene oxide (GO) and *Moringa oleifera* seed oil (MOSO) into a gelatin matrix to create polymer films and evaluate their potential as active packaging materials. The properties of these films were evaluated using structural, thermal, mechanical, optical, and physicochemical methods to determine their suitability for food packaging applications. The results showed that GO and MOSO were homogeneously dispersed in the gelatin matrix, forming colloidal particles (around 5 μm in diameter). The addition of GO increased opacity by approximately 20 times the base value while MOSO affected light transmittance without impacting opacity. Mechanical properties were affected differently, GO acted as a crosslinking agent reducing elongation and increasing tensile strength at break, on the other hand MOSO acted as a plasticizer, making films more plastic increasing elongation a 30%. These effects counteracted each other, and similar behavior was recorded in differential scanning calorimetry. The films exhibited an improved water vapor resistance, which is crucial for food packaging. These findings indicate that the incorporation of GO and MOSO into a gelatin matrix may produce biodegradable polymer films with enhanced properties, suitable for active packaging in the food industry.

KEYWORDS

Biodegradable packaging; graphene oxide; *Moringa oleifera* seed oil; mechanical properties; thermal stability; water vapor resistance; food packaging applications

Nomenclature

GO	Graphene oxide
MOSO	*Moringa oleifera* seed oil
MDSC	Modulated differential scanning calorimeter
SEM	Scanning Electron Microscopy
XRD	X-ray diffraction
TGA	Thermogravimetric Analyzer
ΔE	Total color difference
C	Chroma
h	Tone

1 Introduction

Polymeric materials are widely consumed for the formulation of single-use plastics, specifically in the food industry, where non-degradable plastics are the most commonly used packaging materials [1]. For this reason, the development of novel substitutes is of utmost importance not only to function as a barrier between food products and the environment but also to improve shelf life and preserve organoleptic properties [2]. Active biodegradable materials have been thoroughly researched in recent years [3]. Although significant advances have been achieved, such as new materials, processing methods, and active compounds, there is also a need to assess and evaluate the functional and active properties of these new materials.

Biodegradable polymers are common in nature; collagen, for instance, is the most abundant structural protein and is found in a wide range of animal species [4]. Collagen consists of three peptide chains arranged in a helix; gelatin is obtained from collagen when the bonds between chains are broken, or the chains are partially hydrolyzed [4,5]. Gelatin is mainly known for its role as a food ingredient; nonetheless, it has shown potential as a packaging material due to its availability, low cost, mechanical properties, film-forming capacity, and effectiveness as an oxygen barrier [6]. While gelatin presents great opportunities for food packaging, it also comes with limitations—for example, its highly hydrophilic nature, which means it can swell or dissolve prematurely when in contact with wet foods, such as meats [6]. In this sense, strategies to improve gelatin properties need to be explored. One way to achieve this is to incorporate active or technological compounds to create hydrophobic regions, which could improve water resistance, or add plasticizers to improve mechanical properties [7].

Graphene oxide is a modified form of graphene with functional oxygen groups added to the carbon matrix; in this form, the material can be dispersed in aqueous solutions due to the hydrophilic nature of the functional groups [8]. In addition to its low cost and ease of production, graphene oxide is a known crosslinking agent of macromolecular materials, thanks to its ability to form new bonds between polymeric chains [9]. Previous studies have reported GO enhancing the mechanical properties of polymeric materials, increasing their elongation or tensile strength at break [10]. Even more compelling is that graphene oxide has recently become a relevant material for active packaging research, as it has shown antimicrobial activity and negligible cytotoxicity [11].

Moringa oleifera is widely known for its broad range of applications, such as antimicrobial, insecticidal, or medicinal properties [12]. Moringa oil consists of around 70% oleic acid and contains a significant amount of phytochemicals, such as tocopherols and phenolic acids [13]; it can be obtained by physical extraction from *Moringa oleifera* seeds. This oil has been widely studied, and its components have been linked to several health benefits, such as anticancer and anti-inflammatory properties [14]. The incorporation of moringa seed oil into polymeric matrices exhibits a plasticizing effect [15]; this means that fatty acids and phytochemicals found in moringa seed oil can improve the molecular mobility of polymeric chains. Even more interesting is the ability to easily incorporate this oil into polymeric matrices, as well as the

antimicrobial activity and antioxidant capacity exhibited by these composites [14,16]. Consequently, moringa oil could be a suitable active compound to incorporate in various packaging materials to improve food stability. For example, Cueto Covarrubias et al. demonstrated this potential by maintaining the quality of turkey ham slices after storage in contact with a polymeric film containing MOSO [17].

In this sense, this work aims to improve the properties of gelatin-based polymeric films by incorporating graphene oxide and moringa oil and to evaluate their potential use as active packaging materials. The properties of the obtained films were characterized by structural, thermal, mechanical, optical, and physicochemical methods to determine their suitability for food packaging applications.

2 Materials & Methods

2.1 Materials

Gelatin with a 250 Bloom strength, extracted from bovine sources (moisture content < 4%), was supplied by Factores & Mercadeo (Cartagena, Bolivar, Colombia); graphene oxide (diameter < 5 μm diameter) obtained from Carbon Gates Technology LLC. (Austin, TX, USA), glycerol (99.5%) and glutaraldehyde synthesis solution from Panreac Química (Bogotá, Cundinamarca, Colombia), and pure moringa oil (USDA certified) purchased from Prime Natural (Iztapalapa, Ciudad de Mexico, Mexico) were used for film production.

2.2 Film Preparation

To evaluate the effect of the film components, two concentration levels of GO and MOSO were considered for the formulations, as well as a gelatin control without GO and MOSO. Table 1 shows the mass fractions of all components in the film formulations, where a 2^2 factorial design with three controls was used for a total of seven formulations, each produced in triplicate.

Table 1: Mass fractions of seven film formulations considered in the experimental design

Formulation	Gelatin	Graphene oxide	Moringa oil	Glycerol	Glutaraldehyde
CTR	0.850	0.000	0.000	0.125	0.025
G2	0.830	0.020	0.000	0.125	0.025
M2	0.830	0.000	0.020	0.125	0.025
G1M1	0.830	0.010	0.010	0.125	0.025
G2M1	0.821	0.020	0.010	0.124	0.025
G1M2	0.821	0.010	0.020	0.124	0.025
G2M2	0.813	0.020	0.020	0.123	0.024

Glycerol is a known plasticizer for hydrophilic polymers; therefore, it is necessary to ensure that the obtained films are malleable and stretchable. Glutaraldehyde is a widely used cross-linking agent that can improve the thermal and mechanical stability of gelatin [7].

According to the methodology proposed by [18] to obtain 10 g of film, GO and MOSO were diluted in distilled water and kept under magnetic stirring at room temperature until the compounds were homogenized. Then, gelatin was added and stirred into water (50°C) at a concentration of 2% (w/w) relative to the weight of this polymer. This ratio was maintained for all formulations. After 15 min, glycerol was added as a plasticizer, and after 10 min, glutaraldehyde was added drop by drop using a micropipette. The film-forming solutions were stirred for another 4 h until a homogeneous dispersion was obtained; the solution was then cast onto Teflon trays (15 × 15 cm) and dried in an oven at 50°C for 6 h. The obtained films

were peeled from the trays and conditioned at 53% relative humidity and 25°C for 7 days prior to characterization (Fig. 1). All analyses were performed in triplicate, except for mechanical analyses, which were performed with eight repetitions.

Figure 1: Film preparation process: (a) Film-forming solutions containing graphene oxide; (b) Solution cast on Teflon tray; (c) Films removed from trays after drying

2.3 Film Characterization

2.3.1 Scanning Electron Microscopy (SEM)

The morphology of the films was observed using a scanning electron microscope (FE-SEM, JSM-74101 F, JEOL, Akishima-shi, Japan) with an acceleration voltage of 5.0 kV. Prior to imaging, the films were cryogenically fractured and coated with gold to observe the morphology and dispersion of the components, and then examined at different magnifications.

2.3.2 Optical Microscopy

The sample surface was examined under an optical microscope integrated with a high-definition camera. The obtained microphotographs were analyzed with Image Pro-Plus (v. 5.1) software, as described by Gómez-Contreras et al. [19].

2.3.3 UV-Vis Spectral Characteristics

Spectral characterization was carried out by measuring the normal transmittance of the film samples with a standard configuration in an Evolution 60S UV-visible spectrophotometer (ThermoFisher Scientific). Absorbance was calculated at 600 nm, and transmittance at 450 nm.

2.3.4 X-Ray Diffraction

XRD patterns were recorded using an X-ray diffractometer (D8 Advance ECO, Bruker, USA). Samples were dried inside a desiccator with phosphorus pentoxide and then placed in the sample port and analyzed in a 2θ range of 5°–40°, with Kα radiation from Cu (1.5418 Å) at 40 kV and 25 mA. The degree of crystallinity was calculated from the crystalline peak areas in the obtained diffractograms using OriginLab Software v. 10.1.5.132 [20].

2.3.5 Thermal Properties

To assess the thermal stability of the films, thermal degradation was evaluated in a thermogravimetric analyzer (TGA, Q500, TA Instruments). Measurements were conducted from 30°C to 600°C in an N_2 atmosphere and up to 800°C in an O_2 atmosphere at a rate of 10°C/min.

Thermal first and second-order transitions were evaluated in a modulated differential scanning calorimeter (MDSC) (DSC Discovery series). The analysis conditions were as follows: from −20°C to 150°C with a ramp of 5°C/min, an oscillation amplitude of ±0.32°C and an oscillation period of 60 s.

2.3.6 Moisture Content

Following the method described by Gómez-Contreras et al. [19], the moisture content of the samples was determined by a gravimetric method. Films were conditioned at 56% RH in a desiccator with a sodium bromide oversaturated solution for a week, and 4 × 4 cm sheets were cut and weighed ($M1$) on a Sartorius analytical balance. Sheets were then placed in an oven at 70°C for 45 min and weighed again ($M2$). Moisture content was calculated based on the observed mass difference as described in Eq. (1).

$$Moisture\ (\%) = \frac{M1 - M2}{M1} x\ 100\% \tag{1}$$

2.3.7 Swelling

A gravimetric method was used to calculate the swelling percentage [19]. Dry film samples were weighed and then immersed for 24 h in 20 mL of distilled water. Afterward, excess water on the film surface was eliminated, and samples were weighed once again. To evaluate the expansion of the samples, the thickness was measured with a vernier caliper. All measurements were conducted in triplicate.

2.3.8 Optical Properties

The methodology described by Ordoñez et al. [21] was adapted to determine the color coordinates (L*, a* and b*) in the CIELAB space in a CS-10 colorimeter. Chroma (C*), tone (h*) and total color difference ($\Delta\eth$,) were calculated using a reference sample.

Gloss was calculated according to the ASTM D523 method as adapted by Ortega-Toro et al. in 2017, a flat surface gloss meter (3nh multi-angle YG268, Minolta, Germany) was used to measure superficial gloss at a 60° angle. The obtained results were expressed as gloss units (GU) compared to the highly polished surface of standard black glass with a gloss value of 100 GU.

2.3.9 Mechanical Properties

Following the method used by [22], a digital micrometer (TL 268, TOP EU) with a 0.01 mm precision was used to measure the thickness of the samples. Measurements were taken at three random positions, and a mean was calculated.

Strips of samples (25 × 100 mm) with previously measured thickness were mounted on tensile grips, and an AGS-X 500N precision universal tester (Shimadzu, Kyoto, Japan) was used to obtain strain-stress curves and to calculate tensile strength at break (TS), elastic modulus (EM) and elongation at break (E) according to the ASTM D882 method. Eight replicates were conducted per sample formulation.

2.3.10 Surface Wettability

Water contact angle measurements were conducted by dropping a water droplet on the neat surfaces of the samples. After 60 s, a digital picture was taken with a white background and a 20 cm distance between the droplet and the camera lens. Gonitrans Pro software was used to analyze the pictures and to determine the contact angle; all measurements were conducted in triplicate.

2.3.11 Water Vapor Permeability

Water vapor transmission rate (WVTR) and water vapor permeability (WVP) were evaluated with gravimetric methods and Payne cup setups according to ASTM E96. As described by Cofelice et al. [22], cups were filled with 5 mL of distilled water and covered with circular film samples. They were then placed in desiccators with an oversaturated $MgCl_2$ solution and maintained at 25°C. The cups were periodically weighed (every 1.5 to 24 h) using a Sartorius analytical balance. The weight loss rate [g/h] over time was used to calculate the water vapor permeability (WVP) once the stationary state was achieved. Each sample was measured in triplicate.

$$WVTR = \frac{Weigth\ loss\ rate}{Film\ area} \tag{2}$$

$$WVP = \frac{WVTR}{P_{W1} - P_{W2}} \cdot thickness \tag{3}$$

where P_{W1} and P_{W2} are the water pressure inside and outside the Payne cup, respectively.

2.3.12 Statistical Analysis

All results were analyzed using Statgraphics Plus v. 5.1 software (Manugistics Corp., Rockville, MD, USA). An analysis of variance (ANOVA) was conducted, and the averages were evaluated using Fisher's Least Significant Difference (LSD) test with a 95% confidence level.

3 Results and Discussion

3.1 Scanning Electron Microscopy (SEM)

Cross-sectional micrographs at 350× magnification of all formulated samples are shown in Figs. 2 and 3. The gelatin control exhibits a clean and consistent structure, indicating that a homogeneous gelatin matrix was obtained. The formulation with only GO showed small clusters (around 5 µm in diameter) embedded in the gelatin matrix; comparable results were observed by Barra et al. [23] when incorporating reduced graphene oxide into a chitosan matrix. On the other hand, the incorporation of MOSO generated small wrinkles and micro-oil droplets (around 3 µm in diameter) in the film. The formation of droplets stabilized by the polymer chains has been reported when incorporating MOSO in polymeric matrices such as PVC, as noted by Amina et al. [16]. In formulations containing both MOSO and GO, clusters and droplets are observed dispersed within the matrix. This microstructural analysis concludes that while a large portion of the incorporated GO and MOSO appears to be homogeneously dispersed and interacting with the gelatin chains, another portion of these compounds forms colloidal particles dispersed within the film matrix.

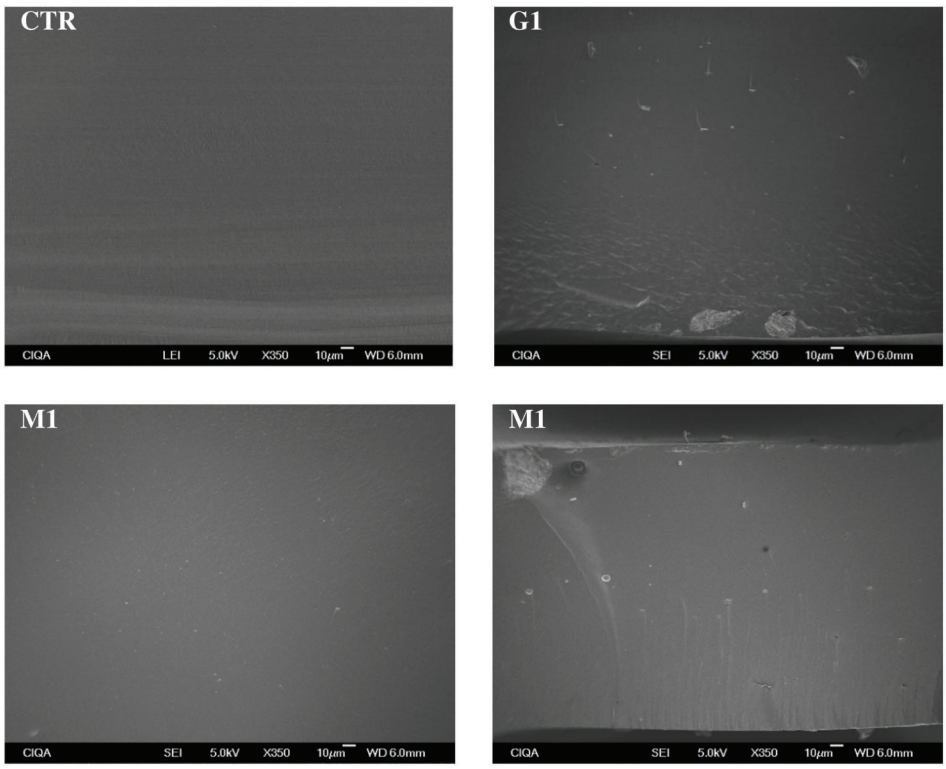

Figure 2: (Continued)

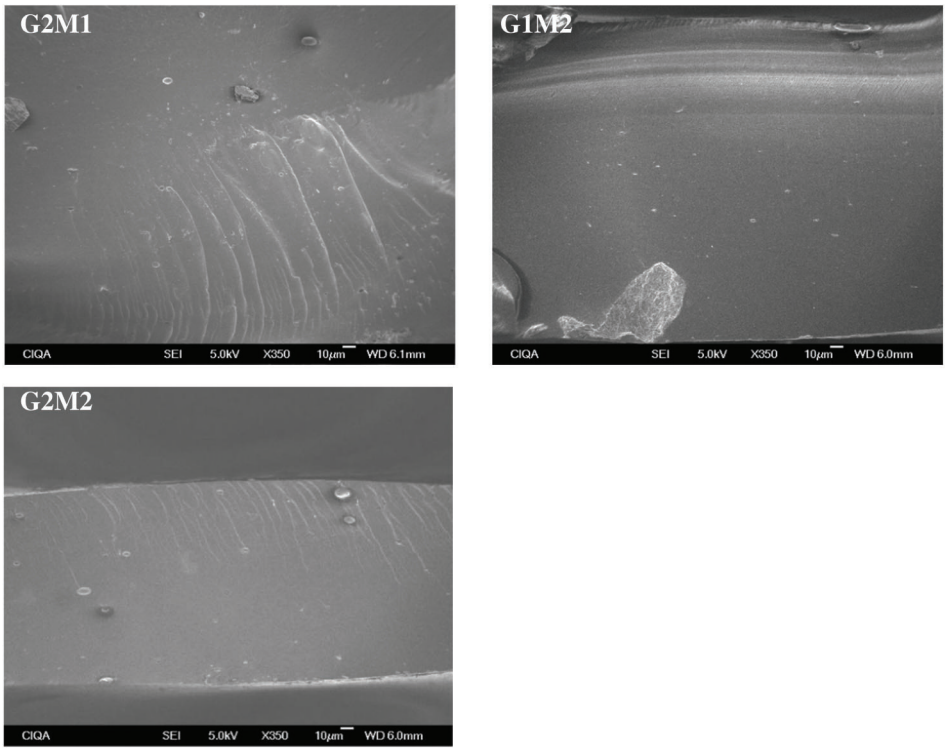

Figure 2: Cross-sectional SEM micrographs of the studied films at 350× magnification

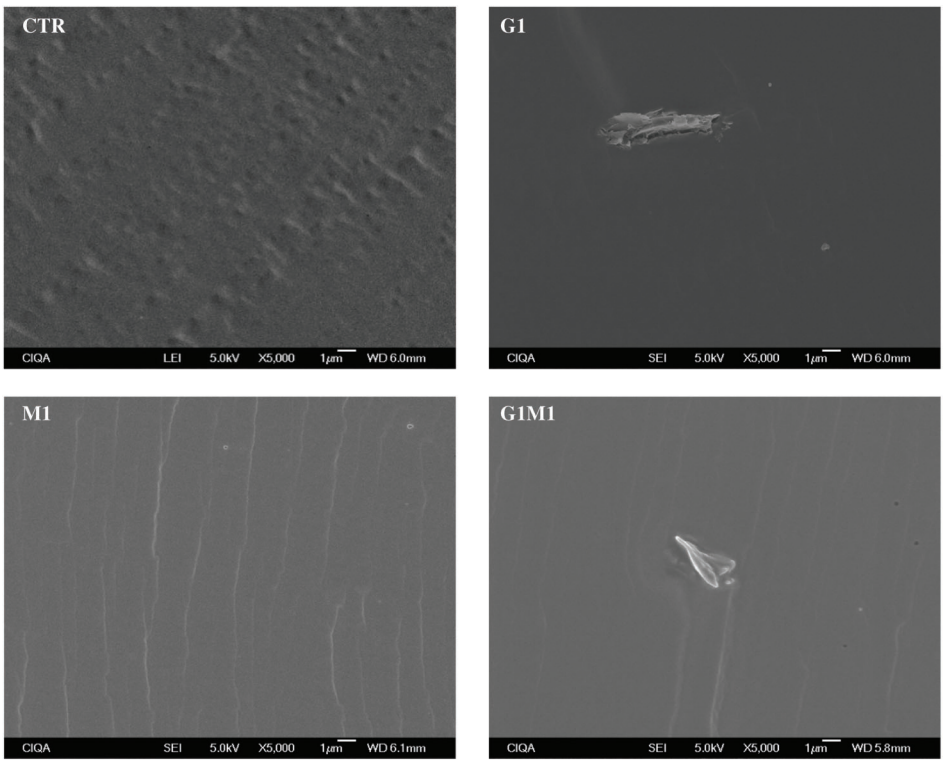

Figure 3: (Continued)

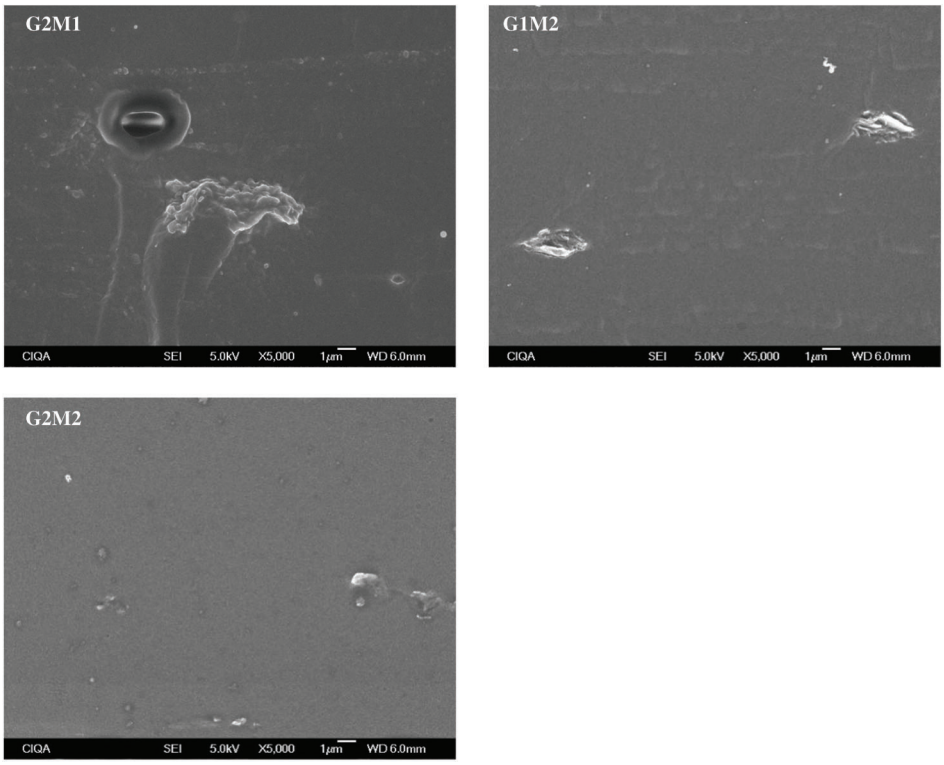

Figure 3: Cross-sectional SEM micrographs of the studied films at 5000× magnification

3.2 Optical Microscopy

The surface morphology of the studied films, obtained by optical observations at 40× magnification, is shown in Fig. 4. As expected for the control film, a smooth and even surface was observed. In contrast, formulations incorporating GO presented an uneven and intricate topography, indicating that the polymeric matrix was not as homogeneous as the control film [24]; this observation aligns with the presence of clusters detected in SEM. Interestingly, despite the polarity differences between gelatin and MOSO, the incorporation of MOSO did not affect the surface topography as drastically as GO did. When both GO and MOSO were added to the gelatin matrix, the surface became more intricate but less uneven than when only GO was added, suggesting that these compounds are interacting with each other.

3.3 UV-Vis Spectral Characteristics

Opacity (600 nm) and transmittance (450 nm) values are displayed in Table 2. For the control films, the opacity was 1.88%, as expected for a homogeneous and translucent film that does not affect light absorption. GO drastically increased opacity, as expected due to its heavily opaque nature; similar results were observed by Frigols et al. [11], where even a small amount of this compound turned alginate films dark. MOSO alone did not significantly affect opacity, indicating that the compound did not modify light absorption.

Results of light transmittance at 450 nm indicated that all formulations experienced a decrease in this property when compared to the 43% measured for the control films. As expected, GO significantly affected transmittance, with a clear relationship observed between increased GO concentration and decreased transmittance. MOSO also decreased transmittance but to a lesser extent. The fact that MOSO decreased transmittance but did not affect opacity values indicates the presence of colloidal interfaces capable of refracting light. This finding is consistent with the capacity of proteins to emulsify MOSO [25], forming the small droplets observed in SEM images, with diameters ranging from 1 to 3 μm.

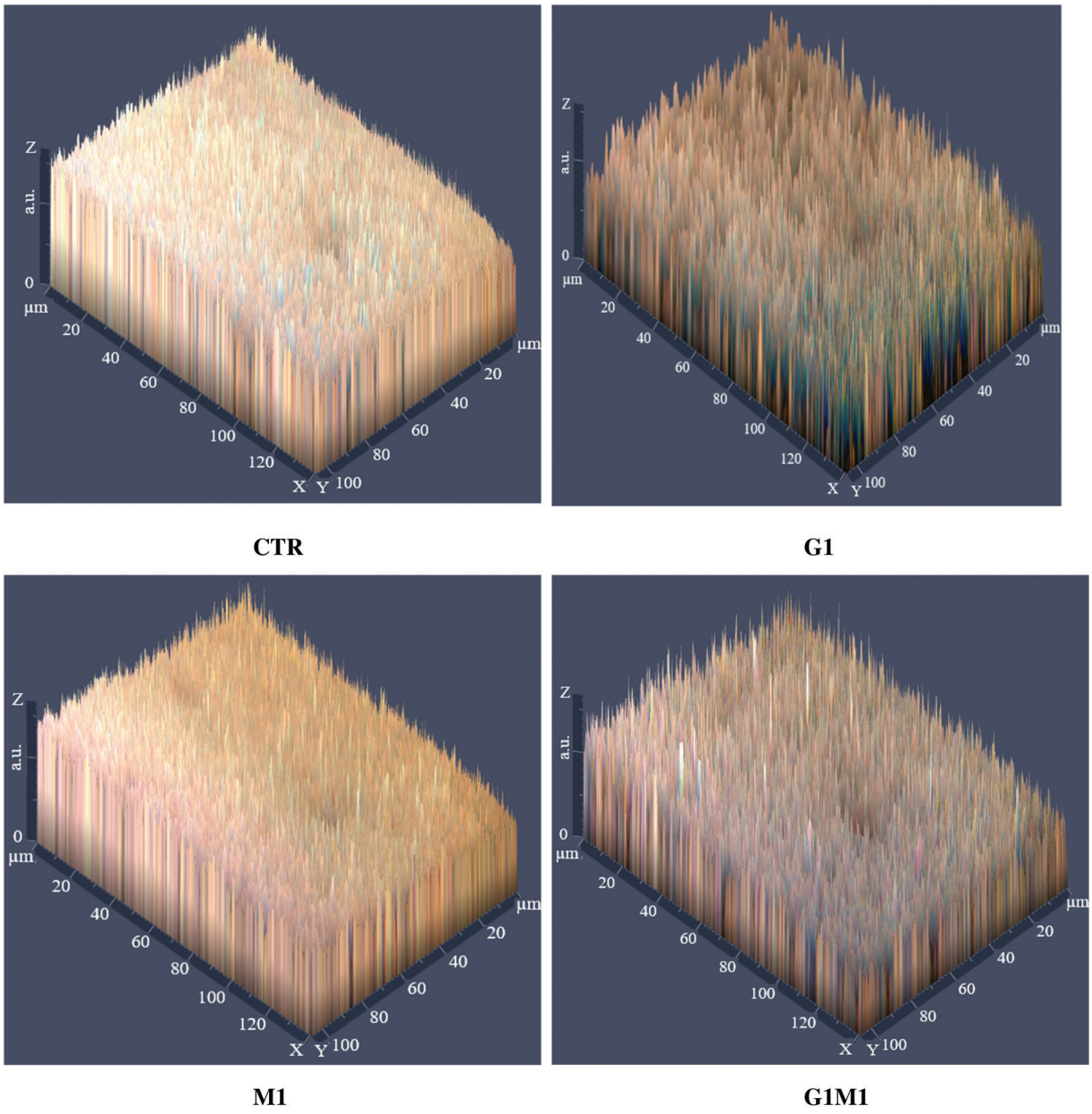

Figure 4: Surface optical micrographs of the studied films at 40× magnification

Table 2: Opacity and transmittance of formulated films

Formulation	Opacity at 600 nm (%)	Transmittance at 450 nm (%)
CTR	1.9 ± 4.0^{a}	0.43 ± 0.02^{a}
G2	37 ± 2^{c}	0.08 ± 0.02^{de}
M2	1.8 ± 2.0^{a}	0.24 ± 0.02^{b}
G1M1	61 ± 3^{b}	0.15 ± 0.02^{c}

(Continued)

Table 2 (continued)

Formulation	Opacity at 600 nm (%)	Transmittance at 450 nm (%)
G2M1	38 ± 3^{c}	0.06 ± 0.02^{e}
G1M2	60 ± 2^{b}	0.12 ± 0.02^{cd}
G2M2	30 ± 4^{d}	0.10 ± 0.02^{d}

Note: Different superscript letters within the same column indicate significant differences among formulations ($p < 0.05$).

3.4 X-Ray Diffraction

The obtained X-ray diffractograms of the film samples are shown in Fig. 5. The CTR and M2 samples only showed a single broad halo located around a 2θ angle of 20°. A single halo is characteristic of amorphous materials, and the observed peak corresponds to previous observations in gelatin matrices [5]. These results also indicate that MOSO did not increase the crystallinity of the polymeric matrix, acting as a plasticizing agent. When low molecular weight molecules such as the fatty acids and phytochemicals contained in MOSO (13) are added to a polymer matrix, they can reduce friction between macromolecules [26]. In the case of gelatin, this could increase the molecular mobility of the peptide chains.

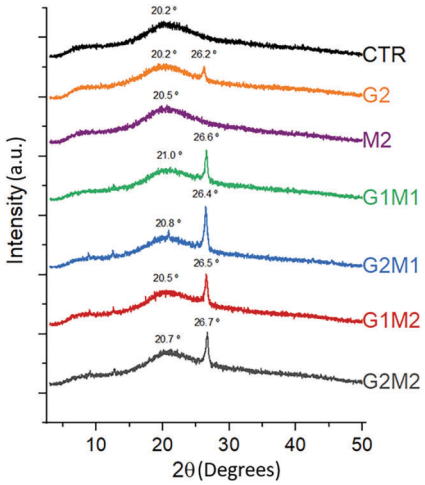

Figure 5: X-ray diffractograms of formulated films

In contrast, formulations with GO alone and with MOSO presented a sharp peak around a 2θ angle of 26° along with the broad peak of the gelatin control; this new peak corresponds to the main diffraction of pure GO at 27° [27]. Interestingly, when MOSO is added, this crystalline peak becomes larger, indicating an increase in the material's crystallinity. The oil's plasticizing effect promotes the molecular mobility of GO, allowing it to reorganize and form larger crystals [28].

The degree of crystallinity was measured, and as can be observed in Fig. 5, only formulations containing GO develop new crystalline peaks, indicating a new crystalline region. The degree of crystallinity values was 3.88%, 7.02%, 5.70%, 6.12%, and 6.25%, corresponding to G2, G1M1, G2M1, G1M2, and G2M2, respectively. The increase in crystallinity in the polymeric matrices compared to G2 samples suggests that GO and MOSO, when mixed, are actively interacting with each other.

3.5 Thermal Properties

Thermal properties are summarized in Table 3. The glass transition for the gelatin control was recorded in the expected range at 79°C [7]. The glass transition temperature (Tg) was significantly modified by the incorporation of both MOSO and GO. MOSO functioned as a plasticizer, drastically lowering the Tg of the gelatin matrix [15]; the lowest Tg of 50°C was observed when MOSO was incorporated alone. In contrast, graphene oxide alone slightly increased Tg, suggesting once again that it could be acting as a crosslinking agent [11], which confirms the observations from the XRD analysis. The crosslinking and plasticizing effects of each agent were evaluated in formulations containing both MOSO and GO, where both effects counteracted each other. When GO and MOSO were both present in a formulation, Tg values only increased at high concentrations of GO, indicating that MOSO inhibited the crosslinking capacity. This effect could suggest that fatty acids present in MOSO may bind with the GO active sites, reducing the capacity of GO to interact with peptide chains. DSC thermograms, displayed in Fig. 6, show similar behavior in all formulations with a smooth glass transition without marked slopes; nonetheless, the G2 formulation containing only MOSO in the gelatin matrix modified the glass transition behavior, now showing a quick and pronounced transition.

Table 3: Thermal properties of formulated films, water release temperature (T_w), initial peak of degradation temperature (T_{Peak}), and maximum degradation peak temperature (T_{Max})

Formulation	Glass transition temperature (°C)	T_w (°C)	T_{Peak} (°C)	T_{Max} (°C)
CTR	79 ± 0.2^{c}	117.5 ± 0.2^{a}	247.9 ± 0.2^{e}	314.74 ± 0.2^{c}
G2	82.75 ± 0.13^{b}	—	245.6 ± 0.2^{f}	311.1 ± 0.2^{d}
M2	50.07 ± 0.08^{e}	98.1 ± 0.2^{c}	261.3 ± 0.2^{a}	320.2 ± 0.2^{b}
G1M1	73 ± 0.2^{d}	109.0 ± 0.2^{b}	252.2 ± 0.2^{c}	320.8 ± 0.2^{b}
G2M1	86.36 ± 0.03^{a}	116.3 ± 0.2^{a}	250.4 ± 0.2^{d}	323.8 ± 0.2^{a}
G1M2	79.2 ± 0.2^{c}	118.1 ± 0.2^{a}	255.3 ± 0.2^{b}	311.7 ± 0.2^{d}
G2M2	$84.3 \pm 1.4a^{b}$	117.6 ± 0.2^{a}	252.9 ± 0.2^{c}	303.6 ± 0.2^{e} 319.8 ± 0.2^{b}

Note: Different superscript letters within the same column indicate significant differences among formulations ($p < 0.05$).

Thermogravimetric analysis revealed that most of the formulated films retained some moisture; the temperature at which water is released (T_w) was around 117°C for most formulations, while the Tw value decreased to 98°C for the M2 formulation, indicating that the plasticizing interactions of water with the polymeric chains were replaced with protein-lipid interactions, leaving water less bound and more likely to leave the gelatin matrix (Fig. 7). An interesting behavior was observed in the G2 formulation, which contains only GO and gelatin. In this case, no Tw or any sign of water loss was observed. A possible explanation could be that the active sites of GO strongly bind water, preventing it from evaporating. However, with the presence of MOSO, this effect is lost, perhaps as lipids occupy the active sites, preventing water from interacting with GO.

Maximum thermal degradation occurs in two main stages for all films; hence two temperatures are reported, corresponding to the first peak (T_{Peak}) and the maximum degradation peak (T_{Max}). The existence of these two degradation peaks indicates the presence of two different polymeric fractions [21], these fractions exist in all formulations hence the most likely explanation is that glutaraldehyde cross-linking creates a fraction with reduced molecular mobility and less resistance to temperature increases.

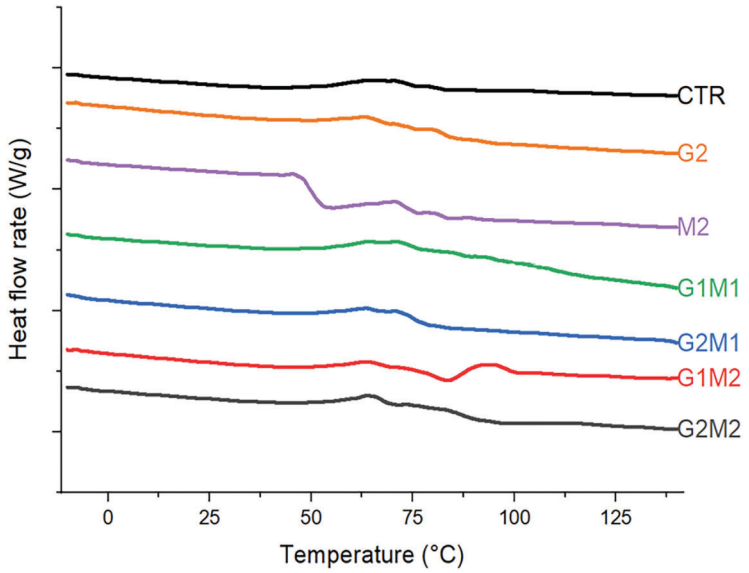

Figure 6: DSC thermograms (reversing heat flow) of formulated films, heat flows from bottom to top

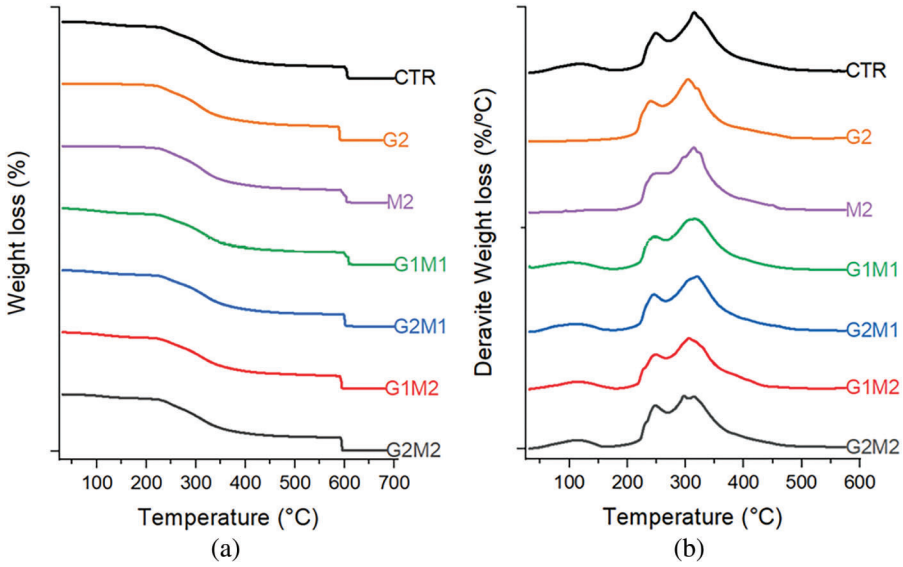

Figure 7: Thermogravimetric analysis non-derivative (a) and derivative (b) of formulated films

3.6 Moisture Content

Table 4 shows the obtained results for moisture content on a dry basis. While the control gelatin and formulations containing GO or MOSO alone showed low moisture content, around 2%–3% after conditioning, the formulations containing both compounds at high concentrations significantly increased moisture retention up to 13%. This high retention could be explained by GO and MOSO forming internal pockets of water; these pockets could form around GO clusters, given GO's hydrophilic nature [29]. However, an additional effect from MOSO must be involved in this phenomenon, since the G2 formulation containing only GO in gelatin did not experience this increase in moisture content. On the contrary, G2 reduced its apparent moisture content, which is consistent with the observed change in TGA, as bound water could not be removed at 70°C.

Table 4: Moisture content and swelling index of formulated films

Formulation	Moisture content (Dry %)	Swelling (%)
CTR	3.6 ± 1.2^{c}	322 ± 9^{ab}
G2	2.0 ± 0.3^{d}	368 ± 38^{a}
M2	2.0 ± 0.4^{d}	315 ± 23^{ab}
G1M1	12.6 ± 0.4^{ab}	349 ± 21^{a}
G2M1	13.3 ± 0.3^{a}	325 ± 35^{ab}
G1M2	13.14 ± 0.10^{a}	325 ± 19^{ab}
G2M2	12.48 ± 0.14^{b}	312 ± 15^{b}

Note: Different superscript letters within the same column indicate significant differences among formulations ($p < 0.05$).

3.7 Swelling

Swelling data are shown in Table 4; although the pronounced differences observed in moisture content, none of the evaluated formulations exhibited significant differences in the swelling index, despite the incorporation of hydrophilic GO.

3.8 Optical Properties

G Gloss and color parameters are summarized in Table 5. Gloss was significantly reduced by the addition of GO; while gelatin tends to be a homogeneous matrix, the addition of GO could partially disrupt its continuous matrix [30]. In contrast, the formulation containing only MOSO (M2) did not affect the gloss, but in formulations with both GO and MOSO, the dulling effect was intensified by the addition of MOSO, once again suggesting strong interactions between these compounds. This could indicate that some MOSO occupies the active sites of GO or that the increased peptide chain mobility allows the formation of crystalline structures.

Table 5: Gloss (UG: unit gloss) and color (L*: Lightness; a*: red-green tones; b*: yellow-blue tones; C: Chroma; h: Hue angle; ΔE: Color Difference) parameters of obtained films

Formulation	Gloss (UG)	Color parameters					
		L*	a*	b*	C	h	ΔE
CTR	63 ± 8^{a}	78.1 ± 1.5^{a}	6.0 ± 0.8^{a}	41 ± 5^{a}	42 ± 5^{a}	82 ± 2^{c}	0
G2	53 ± 7^{ab}	38 ± 3^{d}	-1.1 ± 0.3^{e}	16.8 ± 1.7^{de}	17 ± 2^{d}	94 ± 2^{a}	48 ± 2^{c}
M2	62 ± 6^{a}	55 ± 9^{b}	4.0 ± 0.2^{b}	30 ± 3^{b}	31 ± 4^{b}	101 ± 9^{a}	12 ± 0.5^{a}
G1M1	58 ± 3^{a}	45 ± 3^{bcd}	0.5 ± 0.05^{d}	25 ± 3^{bc}	25 ± 3^{bc}	89.2 ± 0.9^{b}	37 ± 4^{b}
G2M1	33 ± 9^{b}	44.7 ± 0.5^{c}	-1.6 ± 0.04^{f}	18 ± 0.9^{d}	17.7 ± 0.8^{d}	95.4 ± 1.5^{a}	42 ± 3^{ab}
G1M2	42 ± 9^{b}	45.2 ± 1.4^{bc}	0.93 ± 0.08^{c}	24.2 ± 1.0^{c}	23.6 ± 1.0^{c}	87.7 ± 0.6^{b}	38 ± 3^{b}
G2M2	39 ± 8^{b}	37 ± 6^{d}	-2.4 ± 0.4^{g}	14 ± 2^{e}	14 ± 4^{d}	101 ± 5^{a}	50 ± 6^{a}

Note: Different superscript letters within the same column indicate significant differences among formulations ($p < 0.05$).

Similar conclusions can be drawn from the color parameters: lightness was again reduced by GO addition, but not significantly affected by MOSO; this effect is caused by the darkening imparted by GO. The a* parameters changed little, though a slight decreasing trend was observed, indicating that films

turned greener with the addition of GO and MOSO. A similar pattern, but with greater changes, was observed in b*, chroma, and hue parameters, indicating that the tested films were yellower, less saturated, and showed a positive shift in hue angle compared to the gelatin control. Finally, color difference (ΔE) was significantly affected by GO addition and, to a lesser extent, by MOSO.

3.9 Mechanical Properties

The obtained results for thickness and mechanical properties of the film samples can be observed in Table 6. GO's addition to gelatin films significantly reduced elongation (E) and tensile strength (TS) hence turning the films more rigid and brittle. This behavior could be explained by the tendency of GO to function as a cross-linking agent. Grande et al. [8] described this crosslinking on chitosan films and found possible covalent bonds being formed with GO.

Table 6: Mechanical properties of gelatin films with or without graphene oxide and moringa oil at different levels of concentration (1 or 2) and gelatin control

Formulation	Thickness (μm)	Elastic modulus (MPa)	Tensile strength at break (MPa)	Elongation at break (%)
CTR	200 ± 20^{b}	8.6 ± 0.3^{b}	61 ± 8^{a}	10 ± 3^{ab}
G2	280 ± 60^{a}	10.7 ± 0.8^{a}	46 ± 8^{b}	7.5 ± 0.8^{b}
M2	290 ± 40^{a}	7.3 ± 0.8^{c}	55 ± 5^{ab}	13 ± 2^{a}
G1M1	180 ± 30^{b}	9.2 ± 0.8^{ab}	46 ± 7^{b}	4.78 ± 0.4^{c}
G2M1	250 ± 40^{ab}	9.9 ± 0.4^{ab}	42 ± 6^{b}	6 ± 2^{bc}
G1M2	290 ± 50^{a}	7.4 ± 0.6^{c}	39 ± 3^{b}	6.4 ± 0.8^{b}
G2M2	210 ± 20^{ab}	7.6 ± 0.5^{c}	31 ± 5^{c}	14 ± 3^{a}

Note: Different superscript letters within the same column indicate significant differences among formulations ($p < 0.05$).

In contrast, MOSO acted as a plasticizer, as E increased while slightly reducing TS. Similar results were observed by Jarnthong et al. [15], where MOSO plasticized natural rubber compounds and was discussed as a potential non-toxic plasticizer. When GO and MOSO were mixed in the gelatin matrix, a significant reduction in TS was observed. A similar trend was observed for E; however, a slight increase in this property was noted at higher concentrations of both MOSO and GO. This effect could be explained by MOSO bonding with GO, thereby reducing the cross-linked fraction of the peptide chains, which confirms the strong plasticizing capabilities of MOSO described by Jarnthong et al. [15].

3.10 Surface Wettability

Significative differences were observed in the water contact angle, obtained results are shown in Table 7. A base value of 55° was observed in the gelatin control, the sole addition of MOSO greatly reduced the contact angle suggesting the presence of polar groups, GO alone did not significantly decrease the angle, non the less when incorporated alongside MOSO contributed to a further decreased of the contact angle indicating superficial polarity was increased.

3.11 Water Vapor Permeability

Water vapor permeability (WVP) results are shown in Table 7. The formulated films experienced slight changes in WVP compared to the gelatin control; however, all films showed WVP values between 1.1 and 2.1 g·mm/KPa·h·m^2. Despite the non-polar nature of MOSO, the addition of this compound alone did not significantly affect the WVP of the gelatin matrix. In contrast to the observed results in surface

wettability, the addition of GO slightly increased WVP, perhaps as a result of graphene oxide active sites acting as a means of water transport within the polymeric matrix.

Table 7: Water contact angle and water vapor permeability of gelatin films with or without graphene oxide and moringa oil at different levels of concentration and gelatin alone control

Formulation	Contact angle (deg)	WVP (g·mm/Kpa·h·m^2)
CTR	55 ± 3^{b}	1.2 ± 0.3^{cde}
G2	50 ± 7^{b}	1.70 ± 0.12^{b}
M2	37 ± 5^{c}	1.29 ± 0.07^{d}
G1M1	39 ± 2^{c}	1.07 ± 0.02^{e}
G2M1	31 ± 2^{c}	1.13 ± 0.12^{de}
G1M2	74 ± 6^{a}	2.09 ± 0.11^{a}
G2M2	57 ± 2^{b}	1.52 ± 0.05^{c}

Note: Different superscript letters within the same column indicate significant differences among formulations ($p < 0.05$).

The incorporation of both active compounds generated mixed results, as G1M1, G2M1 and G2M2 formulations did not exhibit considerable changes in WVP compared to the gelatin control, but the G1M2 formulation significantly increased WVP beyond even GO alone.

The observed behavior clearly states that GO and MOSO are interacting with each other, but the results of these interactions differ between the concentrations and ratios of both compounds; considering the evidence that in presence of GO high concentrations of MOSO allowed an increase in crystallinity but an increase in WVP this could indicate that this creates more colloidal particles such as small GO clusters that reduce interaction with peptic chains hence allowing water to diffuse faster through the continuous phase.

4 Conclusions

Graphene oxide and moringa seed oil were successfully incorporated into the gelatin matrix, and homogeneous films were obtained. These films exhibited comparable properties to control films of pure gelatin; graphene oxide exerted a cross-linking effect, while moringa oil functioned as a plasticizer. Both effects competed when both compounds were incorporated, and physicochemical interaction between these compounds is suggested, mainly due to the variations in mechanical and thermal properties. Despite the observation of microstructures (graphene clusters and oil droplets), the structural integrity of the films was not compromised. Although the hydrophilic nature of the gelatin matrix remained largely unchanged by the incorporation of graphene oxide or moringa oil, this material could be used in a multilayer assembly with a polymer of complementary polarity, imparting resistance and reducing water permeability. Further studies are required to evaluate the antimicrobial activity of these films and the optimal concentration of both active components. Additionally, multilayer assemblies with polyesters should be considered to improve water resistance.

Acknowledgement: The authors would like to thank the University of Cartagena and the Centro de Investigación en Química Aplicada for their support in carrying out this work.

Funding Statement: The authors would like to thank the University of Cartagena for funding through the Strengthening Project Acta 048-2023.

Author Contributions: The authors confirm contribution to the paper as follows: study conception and design: María Fernanda Cardona Lunar, Rodrigo Ortega-Toro; data collection: María Fernanda Cardona Lunar, Ramón Ordoñez, Heidi Fonseca Florido, Joaquín Hernández-Fernández; analysis and interpretation of results: María Fernanda Cardona Lunar, Ramón Ordoñez, Heidi Fonseca Florido, Rodrigo Ortega-Toro; draft manuscript preparation: María Fernanda Cardona Lunar, Ramón Ordoñez, Heidi Fonseca Florido, Joaquín Hernández-Fernández, Rodrigo Ortega-Toro. All authors reviewed the results and approved the final version of the manuscript.

Availability of Data and Materials: All data are provided in the paper. Additional information will be provided upon request to the corresponding author.

Ethics Approval: The study does not require approval by an ethics committee.

Conflicts of Interest: The authors declare no conflicts of interest to report regarding the present study.

References

1. Hernández-García E, Vargas M, González-Martínez C, Chiralt A. Biodegradable antimicrobial films for food packaging: effect of antimicrobials on degradation. Foods. 2021;10(6):1256. doi:10.3390/foods10061256.
2. Atarés L, Chiralt A. Essential oils as additives in biodegradable films and coatings for active food packaging. Trends Food Sci Technol. 2016;48(1):51–62. doi:10.1016/j.tifs.2015.12.001.
3. Ordoñez R, Atarés L, Chiralt A. Biodegradable active materials containing phenolic acids for food packaging applications. Compr Rev Food Sci Food Saf. 2022;21(5):3910–30. doi:10.1111/1541-4337.13011.
4. Liu D, Nikoo M, Boran G, Zhou P, Regenstein JM. Collagen and gelatin. Annu Rev Food Sci Technol. 2015;6(1):527–57. doi:10.1146/annurev-food-031414-111800.
5. Merina PD, Suguna PR, Karpuram P, Vijaylakshmi JV, Renuka M. Extraction and characterization of gelatin: a functional biopolymer. Int J Pharm Pharm Sci. 2017;9(9):239–42. doi:10.22159/ijpps.2017v9i9.17618.
6. Luo Q, Hossen MA, Zeng Y, Dai J, Li S, Qin W, et al. Gelatin-based composite films and their application in food packaging: a review. J Food Eng. 2022;313(1):110759. doi:10.1016/j.jfoodeng.2021.110762.
7. Bigi A, Cojazzi G, Panzavolta S, Rubini K, Roveri N. Mechanical and thermal properties of gelatin films at different degrees of glutaraldehyde crosslinking. Biomaterials. 2001;22(8):763–8. doi:10.1016/S0142-9612(00)00236-2.
8. Grande CD, Mangadlao J, Fan J, De Leon A, Delgado-Ospina J, Rojas JG, et al. Chitosan cross-linked graphene oxide nanocomposite films with antimicrobial activity for application in food industry. Macromol Symp. 2017;374(1):1600113. doi:10.1002/masy.201600114.
9. Mittal H, Al Alili A, Morajkar PP, Alhassan SM. Graphene oxide crosslinked hydrogel nanocomposites of xanthan gum for the adsorption of crystal violet dye. J Mol Liq. 2021;323:115034. doi:10.1016/j.molliq.2020.115034.
10. Sarkar SD, Uddin MM, Roy CK, Hossen MJ, Sujan MI, Azam MS. Mechanically tough and highly stretchable poly(acrylic acid) hydrogel cross-linked by 2D graphene oxide. RSC Adv. 2020;10(18):10949–58. doi:10.1039/D0RA00678E.
11. Frígols B, Martí M, Salesa B, Hernández-Oliver C, Aarstad O, Ulset AST, et al. Graphene oxide in zinc alginate films: antibacterial activity, cytotoxicity, zinc release, water sorption/diffusion, wettability and opacity. PLoS One. 2019;14(3):e0212819. doi:10.1371/journal.pone.0212819.
12. Ali GH, El-Taweel GE, Ali MA. The cytotoxicity and antimicrobial efficiency of *Moringa oleifera* seeds extracts. Int J Environ Stud. 2004;61(6):699–708. doi:10.1080/0020723042000189877.
13. Cervera-Chiner L, Pageo S, Juan-Borrás M, García-Mares FJ, Castelló ML, Ortolá MD. Fatty acid profile and physicochemical properties of *Moringa oleifera* seed oil extracted at different temperatures. Foods. 2024;13(17):2733. doi:10.3390/foods13172733.

14. Shahbaz M, Naeem H, Batool M, Imran M, Hussain M, Mujtaba A, et al. Antioxidant, anticancer, and anti-inflammatory potential of Moringa seed and Moringa seed oil: a comprehensive approach. Food Sci Nutr. 2024;12(9):6157–73. doi:10.1002/fsn3.4312.
15. Jarnthong M, Lopattananon N, Li Y, Yu H, Wang R, Wang Y, et al. Performance of moringa oil as an effective bioplasticizer on static and dynamic mechanical properties of natural rubber vulcanizates. ACS Sustain Chem Eng. 2024;12(16):6440–50. doi:10.1021/acssuschemeng.4c01672.
16. Amina M, Al Musayeib NM, Alarfaj NA, El-Tohamy MF, Orabi HE, Bukhari SI, et al. Exploiting the potential of Moringa oleifera oil/polyvinyl chloride polymeric bionanocomposite film enriched with silver nanoparticles for antimicrobial activity. Int J Polym Sci. 2019;2019:1–9.
17. Cueto Covarrubias LA, Valdez Solana MA, Avitia Domínguez C, Téllez Valencia A, Meza Velázquez JA, Sierra Campos E. Characterization of *Moringa oleifera* seed oil for the development of a biopackage applied to maintain the quality of turkey ham. Polymers. 2024;16(1):132. doi:10.3390/polym16010132.
18. Ooi SY, Ahmad I, Amin Mohd CIM. Cellulose nanocrystals extracted from rice husks as a reinforcing material in gelatin hydrogels for use in controlled drug delivery systems. Ind Crops Prod. 2016;93(10):227–34. doi:10.1016/j.indcrop.2015.11.082.
19. Gómez-Contreras P, Contreras-Camacho M, Avalos-Belmontes F, Collazo-Bigliardi S, Ortega-Toro R. Physicochemical properties of composite materials based on thermoplastic yam starch and polylactic acid improved with the addition of epoxidized sesame oil. J Polym Environ. 2021;29(10):2784–98. doi:10.1007/s10924-021-02119-0.
20. Andrade J, González-Martínez C, Chiralt A. Effect of phenolic acids on the properties of films from poly(vinyl alcohol) of different molecular characteristics. Food Packag Shelf Life. 2021;29(3):100711. doi:10.1016/j.fpsl.2021.100711.
21. Ordoñez R, Atarés L, Chiralt A. Physicochemical and antimicrobial properties of cassava starch films with ferulic or cinnamic acid. LWT. 2021;144(4):111242. doi:10.1016/j.lwt.2021.111242.
22. Cofelice M, Cuomo F, Chiralt A. Alginate films encapsulating lemongrass essential oil as affected by spray calcium application. Colloids Interfaces. 2019;3(3):58. doi:10.3390/colloids3030058.
23. Barra A, Ferreira NM, Martins MA, Lazar O, Pantazi A, Jderu AA, et al. Eco-friendly preparation of electrically conductive chitosan-reduced graphene oxide flexible bionanocomposites for food packaging and biological applications. Compos Sci Technol. 2019;173:53–60. doi:10.1016/j.compscitech.2019.01.027.
24. Bohórquez-Ayala M, Rojano-Quiroz D, González-Cuello R, García-Zapateiro L, Ortega-Toro R. Application of modified vegetable oil for improvement of biodegradable materials based on thermoplastic starch and polylactic acid. Rev Mex Ing Quim. 2021;20(1):423–33. doi:10.24275/rmiq/Poly2164.
25. Makiej A, Hochór Z, Smułek W, Kaczorek E. The bioactivity and physicochemical properties of emulsions based on tamanu, moringa, and inca inchi oils. Foods. 2024;13(1):62. doi:10.3390/foods13010062.
26. Mohamed SAA, El-Sakhawy M, El-Sakhawy MAM. Polysaccharides, protein and lipid-based natural edible films in food packaging: a review. Carbohydr Polym. 2020;238(2):116178. doi:10.1016/j.carbpol.2020.116178.
27. Aragaw BA. Reduced graphene oxide-intercalated graphene oxide nano-hybrid for enhanced photoelectrochemical water reduction. J Nanostructure Chem. 2020;10(1):9–18. doi:10.1007/s40097-019-00324-x.
28. Kumar NSK, Lalge R, Suryanarayanan R. Time and temperature dependence of drug crystallization—the role of molecular mobility. Mol Pharm. 2024;21(11):5880–91. doi:10.1021/acs.molpharmaceut.4c00935.
29. Wang S, Zhang Y, Abidi N, Cabrales L. Wettability and surface free energy of graphene films. Langmuir. 2009;25(18):11078–81. doi:10.1021/la901402f.
30. Ordoñez R, Atarés L, Chiralt A. Properties of PLA films with cinnamic acid: effect of the processing method. Food Bioprod Process. 2022;3(3):25–33. doi:10.1016/j.fbp.2022.02.002.